PAPER

Check for updates

A lung/liver-on-a-chip platform for acute and chronic toxicity studies†

David Bovard, [iD] * Antonin Sandoz, Karsta Luettich, Stefan Frentzel, Anita Iskandar, [iD] Diego Marescotti, Keyur Trivedi, Emmanuel Guedj, Quentin Dutertre, Manuel C. Peitsch [iD] and Julia Hoeng

The merging of three-dimensional *in vitro* models with multi-organ-on-a-chip (MOC) technology has taken *in vitro* assessment of chemicals to an unprecedented level. By connecting multiple organotypic models, MOC allows for the crosstalk between different organs to be studied to evaluate a compound's safety and efficacy better than with single cultures. The technology could also improve the toxicological assessment of aerosols that have been implicated in the development of chronic obstructive pulmonary disease, asthma, or lung cancer. Here we report the development of a lung/liver-on-a-chip, connecting in a single circuit, normal human bronchial epithelial (NHBE) cells cultured at the air–liquid interface (ALI), and HepaRG™ liver spheroids. Maintenance of the individual tissues in the chip increased NHBE ALI tissue transepithelial electrical resistance and decreased HepaRG™ spheroid adenosine triphosphate content as well as cytochrome P450 (CYP) 1A1/1B1 inducibility. CYP inducibility was partly restored when HepaRG™ spheroids were cocultured with NHBE ALI tissues. Both tissues remained viable and functional for 28 days when cocultured in the chip. The capacity of the HepaRG™ spheroids to metabolize compounds present in the medium and to modulate their toxicity was proven using aflatoxin B1 (AFB1). AFB1 toxicity in NHBE ALI tissues decreased when HepaRG™ spheroids were present in the same chip circuit, proving that the HepaRG™-mediated detoxification is protecting/decreasing from AFB1-mediated cytotoxicity. The lung/liver-on-a-chip platform presented here offers new opportunities to study the toxicity of inhaled aerosols or to demonstrate the safety and efficacy of new drug candidates targeting the human lung.

Introduction

The human respiratory system supplies every cell in the body with oxygen and removes carbon dioxide accumulated in the blood. Because of its direct exposure to the air, this organ is also the primary target of airborne pollutants or pathogens. Exposure to environmental aerosols, such as smoke from cigarettes or biomass, was demonstrated to cause chronic obstructive pulmonary disease (COPD), asthma, or lung cancers.[1] The toxicological assessment of aerosols responsible for the development of these diseases requires models that closely mimic human physiology. Animal models have been widely used to study the effects of inhaled toxicants on the lung,[2] but animals express and regulate genes or proteins differently from humans; thus, the data obtained in animal studies cannot be entirely and straightforwardly extrapolated to humans.[3] During the last decade, new *in vitro* models have been developed with an increased level of complexity and physiological features that better reflect the complex mechanisms in specific organs of the human body.[4] Lung *in vitro* models have also benefited from these technological advances. By culturing human primary lung cells at the air–liquid interface (ALI), the cells formed a three-dimensional (3D) epithelium closely mimicking the human lung epithelium.[5] This model has provided opportunities to study more complex physiological processes, such as the differential response of COPD and normal bronchial epithelium to air pollution,[6] or the interaction between a pathogen and the epithelium.[7] More recently, organ-on-a-chip technology, the combination of *in vitro* models with a micro-engineered environment,[8] has facilitated the development of advanced *in vitro* lung models recreating not only the morphology of the lung epithelium but also its physical movement, which modulates epithelial permeability.[9–11]

A single-organ-on-a-chip model is useful to study disease mechanisms in a particular organ but is likely to be insufficiently robust to predict the complex organ crosstalk

PMI R&D, Philip Morris Products S.A., Quai Jeanrenaud 5, CH-2000 Neuchâtel, Switzerland

occurring in the human body. In the context of inhaled compounds, these will first be absorbed by the lung tissue and partially metabolized by cytochrome P450 (CYP) enzymes, generating new metabolites. The small subset of CYP enzymes expressed in the lung would produce only a small portion of all metabolites that would have been produced by other CYPs expressed in other organs.[12] The liver expresses around 30 CYP enzymes out of the 57 identified in humans, thus playing a critical role in compound metabolism.[13] Compounds or metabolites coming from the lung will reach the liver and be transformed into new metabolites. Consequently, the potential toxicity or side effects of these additional metabolites cannot be evaluated adequately using a single-organ-on-a-chip model. To address this issue, different groups have developed various "multi-organ-on-a-chip" (MOC) models combining several organs on one single system (chip).[14–16] These platforms generally connect one (or more) organ(s) with, in most cases, a liver compartment, which is known to be the primary organ for compound metabolization.[17–19]

To better evaluate the potential toxicity of inhaled compounds, we developed a system connecting a 3D organotypic bronchial model with liver spheroid cultures to produce a lung/liver-on-a-chip. The incorporation of a liver model aims to accurately test not only the potential toxicity of the inhaled parent compounds but also that of their metabolites, which may alter the toxicity profile of the administered compounds.[20] Various *in vitro* liver models have been developed in recent years using primary cells or cell lines, such as HepaRG™ and HepG2, either in 2D or 3D conformation.[21] Our 3D liver spheroid model was built using human HepaRG™, which is considered a good hepatic model, as it exhibits high and stable secretion of albumin and metabolic capacity.[22–25] Multiple studies have shown that the toxicity of the anti-tuberculosis agent isoniazid,[26] acetaminophen,[27] or aflatoxin B1 (AFB1)[28] could be predicted accurately using 3D liver spheroid models. For the lung/liver-on-a-chip system, the 3D organotypic bronchial culture was prepared using normal human bronchial epithelial (NHBE) cells cultured at the ALI. These NHBE ALI cultures have been used previously in single, static culture to assess the effects of exposure to cigarette smoke,[29] nanoparticles,[30] and therapeutic agents, such as roflumilast[31] or ozone.[32]

The macro-format chip developed here was made from a biocompatible and non-absorbent material that enables coculture of NHBE ALI and HepaRG™ spheroid cultures. The chip design was expected to be suitable for acute and chronic aerosol exposure studies. Using an extensive array of assays covering morphological, functional, and viability markers, the stability and functionality of both cultures in monoculture and coculture configurations were demonstrated for 28 days. The crosstalk between the two cultures was further demonstrated using AFB1 as an example toxicant. We showed that AFB1 toxicity was reduced in the presence of the HepaRG™ spheroid culture. The lung/liver-on-a-chip platform described here will be useful to predict the safety of inhaled compounds.

Experimental procedures

Human 3D bronchial epithelial cultures

We prepared NHBE ALI tissues following a procedure described by STEMCELL Technologies (PneumaCult™ Medium, Document #29252; STEMCELL Technologies, Vancouver, Canada). Briefly, NHBE cells (Lonza, Basel, Switzerland) were cultured in T75-flasks using PneumaCult™-EX PLUS medium (STEMCELL Technologies) at 37 °C with 5% CO_2 and 90% relative humidity. Once the cells were 80% confluent, they were detached from the flask using trypsin–EDTA (Lonza), and 50 000 cells were seeded on a collagen I-coated Transwell® insert (Corning®, Corning, NY, USA). Both apical and basal sides of the inserts were filled with PneumaCult™-EX PLUS medium and maintained for three days. Subsequently, the culture was airlifted by removing the apical medium; the basal medium was replaced with the PneumaCult™-ALI medium (STEMCELL Technologies). Tissues were used for experiments starting from day 28 after the airlift.
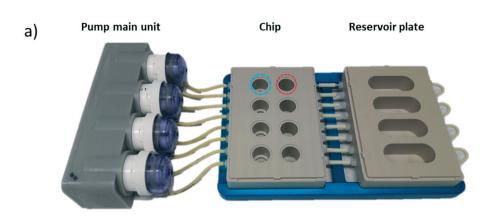
HepaRG™ spheroid cultures

Cryopreserved and differentiated HepaRG™ cells (ThermoFisher Scientific, Waltham, MA, USA) were thawed in William's E medium containing Thaw, Plate & General Purpose Supplement (Thermo Fisher Scientific). Spheroids composed of 12 500 cells were prepared by diluting the 10 million cells present in the cryopreserved vial with 80 mL of William's E medium and seeding 100 μL of this cell suspension into each well of an ultra-low adhesion 96-well plate (Corning). The 96-well plates were kept in the incubator at 37 °C for four days before medium replacement. On the fourth day, cells formed dense aggregates with a visible extracellular matrix confirming spheroid formation. Thereafter, the cell culture medium was renewed every two to three days. Spheroids were used once mature, approximately one week after thawing HepaRG™ cells.
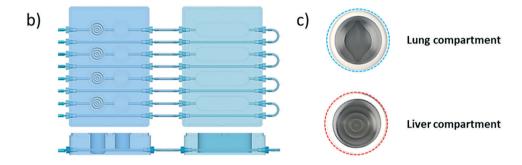
The impact of the PneumaCult™-ALI medium on the HepaRG™ tissues was evaluated by switching spheroids to the PneumaCult™-ALI medium once mature. William's E medium present in the wells of the ultra-low adhesion 96-well plate was removed and replaced with prewarmed PneumaCult™-ALI medium. Medium was renewed every two or three days.

Development and maintenance of the lung/liver-on-a-chip

The chip we developed is composed of four parts: a fluidic plate, reservoir plate, pump unit, and smartphone (Fig. 1). Both plates, the fluidic and reservoir plate, are made from polyetheretherketone (PEEK), an autoclavable material and inert thermoplastic used to develop medical implants.[33] We selected this material for its biocompatibility and because we found it to be non-absorbent for small molecules, such as nicotine, a significant advantage compared with other devices made from polydimethylsiloxane (PDMS), which particularly absorb hydrophobic molecules.[34] Long-term maintenance of
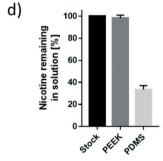
Fig. 1 The lung/liver-on-a-chip platform. a) A photograph of the chip system comprising the pump main unit with four pump heads, the PEEK chip, and the reservoir plate. b) A schematic view of the chip comprising four circuits is shown; each circuit includes two compartments to house the lung and liver tissues, respectively. The cross-section schemas of the plates show the path of the tubes and channels and the relative depth of each well. c) A close-up view of the two compartments showing the groove pattern on the bottom of the wells. d) Effect of chip materials on absorption of nicotine. A solution of 10 mM nicotine in phosphate-buffered saline (PBS) was kept in the wells of the chips made from PEEK or PDMS for eight hours before it was collected. The concentrations of nicotine were then measured using liquid chromatography coupled to high-resolution accurate mass spectrometry. Nicotine concentrations remaining in solution are expressed as % relative to the stock solution. Data are presented as mean ± SEM. $N = 3$. PEEK: polyetheretherketone; PDMS: polydimethylsiloxane.

3D tissues or evaluation of compound toxicity requires the use of a non-absorbent material to keep the level of medium constituents, secreted metabolites, or injected drugs stable over time.[35] Indeed, the concentration of nicotine – a small, hydrophobic molecule[36] – remained similar to the initial stock concentration, even after an eight-hour incubation in the PEEK chip (Fig. 1d). Using a PDMS chip of the same design, the nicotine concentration decreased by 70% following the same incubation period. The fluidic plate (plate dimension: 85.5 × 127.5 cm; standard multi-well plate dimension) has four circuits; each circuit comprises two wells connected by a channel (with a diameter of 2.5 mm) and has a minimum volume of 2.5 mL (the minimum volume refers to the volume needed to ensure that the basal surface of the Transwell® insert is submerged in the medium). For long-term culture (e.g., for 28 days), a larger total volume of medium is needed to ensure that cells are nourished sufficiently. Consequently, for our 28-day experiments, the fluidic plate was connected to a second plate (reservoir plate, Fig. 1a). The reservoir plate comprises four reservoirs used to increase the total volume of medium in the chip up to 9 mL. The pump unit (Fig. 1a) is composed of four peristaltic pumps and four

Bluetooth controllers sealed in a waterproof box. Once the fluidic chip is connected to the pump unit, the whole system can be maintained in a standard cell culture incubator; the pump has a single power cable exiting the rear access of the incubator. The medium flow-rate and flow-direction in each circuit can be controlled using a smartphone application *via* a Bluetooth connection, even when the incubator door is closed.

For a given circuit, one well is available for the NHBE ALI tissue (or any tissue grown on a Transwell® insert), and the other is available for the HepaRG™ spheroids (Fig. 1b). The compartment (well) for the lung cultures has a small cavity on the bottom (Fig. 1c), above which the culture insert is centrally positioned. On the bottom of the liver compartment, small grooves (three concentric grooves with a depth of 1 mm, Fig. 1b) segregate the spheroids and prevent the formation of spheroid aggregates.

Chip operation

To prevent adhesion of the HepaRG™ spheroids to the plate, we coated the wells housing the spheroids with a solution of 5% poly(2-hydroxyethyl methacrylate) (Sigma, Buchs, Switzerland) diluted in pure ethanol. Prior to use, each circuit was run for 30 minutes with the PneumaCult™-ALI medium in a CO_2 incubator to prewarm the plate and medium. NHBE ALI tissues and HepaRG™ spheroids were subsequently transferred to the fluidic chip, and the fluidic chip was connected to the pump main unit. The flow rate was set at 150 μL min^{-1} for all experiments. The medium in each circuit was renewed every two or three days.

The effect of chip materials on compound absorption

Nicotine (Sigma) was diluted in 6 mL PBS to a final concentration of 10 mM. Of this stock solution, 3 mL was then added to one circuit of the chip and incubated for eight hours at 4 °C to prevent evaporation of the solution. The other 3 mL of the nicotine stock solution was kept in a tube at 4 °C for the same duration.

To measure the nicotine concentration, we diluted the samples containing the nicotine and mixed the diluted solution with d3-nicotine, an internal standard. Nicotine was measured by high-performance liquid chromatography coupled to high-resolution accurate mass spectrometry using a calibration curve of eight standards. Full quantitation was based on the isotopic ratio between labeled and unlabeled nicotine.

Histological assessment of human 3D bronchial cultures

Briefly, NHBE ALI tissues were washed three times with PBS and fixed for two hours in freshly prepared 4% (w/v) paraformaldehyde (Thermo Fisher Scientific). The fixed culture was separated from the insert by detaching the membrane from the plastic with forceps and cut at the midpoint prior to processing using the ASP300S tissue processor (Leica, Wetzlar, Germany); the two pieces were embedded in one paraffin

block. Paraffin sections of 5 μm thickness were obtained using a microtome and mounted on glass slides. The slides were subsequently transferred to a Leica ST5020 automated slide stainer for staining with hematoxylin, eosin, and Alcian blue. Subsequently, the stained slides were covered with glass coverslips using Leica CV5030 fully automated coverslippers. Digital images were generated using the NanoZoomer 2.0 slide scanner (Hamamatsu Photonics, Hamamatsu, Japan).

Measurement of TEER

Transepithelial electrical resistance (TEER) was measured in NHBE ALI cultures using an EndOhm-6 chamber (WPI, Sarasota, FL, USA) connected to an EVOM™ Epithelial voltohmmeter (WPI), according to the manufacturer's instructions. The value displayed by the voltohmmeter was multiplied by the surface of the inserts (0.33 cm^2) to obtain the resistance value in the total area (ohm × cm^2).

Measurement of CBF

Cilia beating frequency (CBF) was measured in NHBE ALI cultures using an inverted microscope (Zeiss, Oberkochen, Germany) equipped with a 4× objective and a 37 °C chamber and connected to a high-speed camera (Basler AG, Ahrensburg, Germany). Short movies composed of 512 frames recorded at 120 images per second were analyzed using SAVA analysis software (Ammons Engineering, Clio, MI, USA).

Whole-mount staining of human 3D bronchial cultures

To detect the goblet and ciliated cells composing the 3D NHBE ALI tissues, we used antibodies to target specific cell type markers. Tissues were first fixed in 4% (w/v) paraformaldehyde for 15 minutes and then blocked for one hour in a blocking solution (0.5% Triton X-100 [Thermo Fisher Scientific], 5% normal goat serum [Thermo Fisher Scientific] and 2% bovine serum albumin [Thermo Fisher Scientific] in PBS). Tissues were stained with a β-tubulin 4 antibody conjugated to Alexa 647 (Abcam, Cambridge, United Kingdom) or a MUC5AC antibody conjugated to Alexa 550 (Abcam), diluted in PBS with 2% normal goat serum and 1% bovine serum albumin. Finally, nuclei were counterstained with Hoechst (Thermo Fisher Scientific). Images were acquired using the Cell Insight™ CX7 platform (Thermo Fisher Scientific).

Measurement of cell viability

We evaluated the viability of the NHBE ALI tissues and HepaRG™ spheroids using two different measures: the adenosine triphosphate (ATP) content and the number of apoptotic and necrotic cells. ATP in tissues was measured using the CellTiter-Glo® 3D Cell Viability Assay (Promega, Madison, WI, USA). For HepaRG™ spheroids, the tissue with its medium was first transferred into a 96-well white polystyrene microplate before adding the same volume of CellTiter-Glo® reagent. For NHBE ALI tissues, 150 μL CellTiter-Glo® reagent was added to the apical surface. After 30 minutes, 50 μL of

CellTiter-Glo® reagent was transferred into an opaque-walled 96-well plate from the apical surface of the tissues, and luminescence was measured using a FLUOstar Omega plate reader (BMG Labtech, Ortenberg, Germany). Lactate dehydrogenase (LDH) released into the medium was quantified using the Cytotoxicity Detection Kit^{PLUS} (Roche, Basel, CH) following the manufacturer's instructions.

Measurement of metabolism phase 1 gene expression in liver spheroids

For gene expression analysis, RNA was prepared from HepaRG™ spheroids using the miRNeasy Micro kit (QIAGEN, Hilden, Germany). cDNA was prepared using the RT2 First Strand kit and mixed with RT^2 qPCR Mastermix before plating the mix on a Phase I Enzymes RT^2 Profiler PCR Array (QIAGEN). Quantitative PCR was performed using the ViiA™ 7 Real-Time PCR System (Thermo Fisher Scientific). Calculation of gene expression fold-changes relative to tissues in William's E medium was based on the ΔΔCT method originally published by Livak and Schmittgen[37] and performed using the Data Analysis Center from QIAGEN.

Measurement of the CYP enzymatic activity of liver spheroids

The activity levels of CYP1A1/1B1 enzymes (combined) were measured using the P450-Glo™ kit from Promega following the manufacturer's protocol. To induce the activity of CYP1A1/1B1, HepaRG™ spheroids were incubated with 10 nM 2,3,7,8-tetrachlorodibenzo-p-dioxin (TCDD, Sigma) for 48 hours.

Measurement of glucose, lactate, and albumin in the culture medium

The medium in the chip was collected for the measurement of glucose, lactate, and albumin before each medium renewal. The concentration of albumin in the medium was measured using the Human Albumin ELISA Kit (Abcam) following the manufacturer's instructions. Glucose and lactate concentrations in the culture media were measured using the Biosen Glucose and Lactate Analyzer (EKF, Cardiff, United Kingdom).

AFB1 treatment

AFB1 (Sigma) was first diluted in dimethyl sulfoxide to give a 20 mM stock solution. This solution was then diluted 2000 times with the coculture medium to reach a final working concentration of 100 μM. The fluidic chip was first primed with the diluted AFB1 solution. Subsequently, the chip was run as described before (see Experimental procedures: running the chip).

Statistical analysis

P-values were calculated using Student's t-test. The statistical significance thresholds were set at *$p < 0.05$, **$p < 0.05$, and ***$p < 0.005$. Data are expressed as the mean ± standard error of the mean (SEM) unless otherwise specified.

Results

Selecting a coculture medium suitable for the lung and liver cultures

We developed a platform to coculture 3D bronchial (prepared with NHBE cells; NHBE ALI) and liver spheroid tissues (prepared with HepaRG™ cells; HepaRG™ spheroid) in a single chip to increase the complexity and physiological relevance of tissue responses following exposure to inhaled toxicants. The coculture of the two different tissue types required first a suitable coculture medium able to maintain the two tissues together without impairing their key characteristics.

The NHBE ALI tissues, given their primary origin, were particularly sensitive to the medium composition. We chose to first test the NHBE ALI cell culture medium (PneumaCult™-ALI) to coculture the NHBE ALI tissues and HepaRG™ spheroids in the chip. After 10 days in culture with this medium, the performance (viability and metabolic capacity) of HepaRG™ spheroids was assessed. HepaRG™ spheroids had a ~20% higher ATP content (Fig. 2a) and released ~75% less LDH (Fig. 2b) compared with the HepaRG™ spheroids maintained in William's E medium (i.e., the standard medium for growing and maintaining HepaRG™ cells and spheroids). The increase in spheroid ATP levels could be due to the higher glucose concentration in the PneumaCult™-ALI medium (17 mM) versus the William's E medium (11 mM), thus increasing the rate of glycolysis and ATP production.[38,39] The concentrations of LDH, an enzyme secreted by necrotic cells,[40] were strongly reduced when the spheroids were maintained in PneumaCult™-ALI compared with Williams' E medium (Fig. 2b). The reduced LDH release from tissues maintained with the PneumaCult™-ALI might also be caused by the higher glucose concentration present in this medium. Glucose is not only crucial for energy metabolism, it is also essential for the formation of biosynthetic precursor molecules such as nucleic acids, fatty acids and for protein glycosylation. Consequently, glucose-deprived cells become stressed which triggers apoptosis or necrosis.[41] The cells present near the core of the spheroids could have benefited from the higher glucose in the PneumaCult™-ALI medium, which prevented their necrosis.

Morphologically, the spheroids remained similar after 10 days; the HepaRG™ cells formed a dense aggregate surrounded by a visible extracellular matrix without obvious debris in the medium (Fig. 2c). Overall, these three results demonstrated good tissue viability following a 10-day culture in PneumaCult-ALI™ medium. Additionally, we measured the concentrations of albumin to determine if the HepaRG™ cells retained their hepatic properties regardless of the culture medium (Fig. 2d). Albumin production and secretion increased two-fold when the spheroids were maintained in PneumaCult-ALI™ medium relative to spheroids maintained
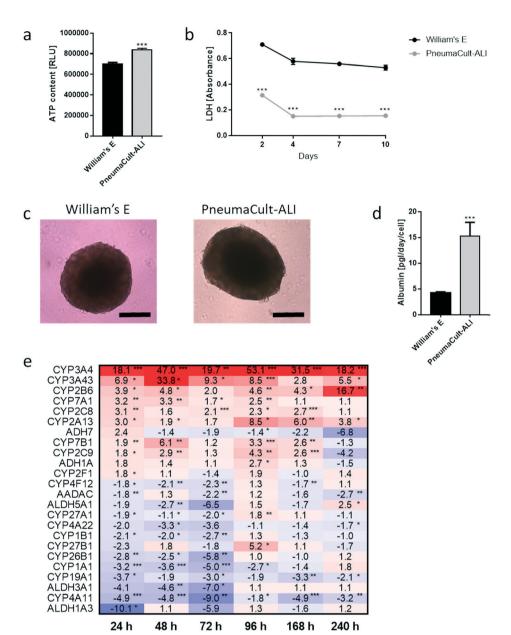
Fig. 2 Effect of PneumaCult™-ALI medium on HepaRG™ spheroid viability, function, and expression of phase 1 metabolism-associated genes. HepaRG™ spheroids were maintained in ultra-low adhesion microplates with either PneumaCult™-ALI or William's E media for 10 days before assessment of a) ATP content, b) LDH release, c) tissue morphology, and d) albumin production. Magnification: 10×. Scale bar: 200 μm. Data are presented as mean ± SEM of eight independent replicates. Student's t-test PneumaCult™-ALI $vs.$ William's E, *** ($p < 0.0005$). e) Heatmap showing the fold-changes in the expression of phase 1 metabolism-associated genes (gene symbols listed on the left) in HepaRG™ spheroids maintained in PneumaCult™-ALI medium compared with those in spheroids cultured in William's E medium over time in culture. Number indicates fold-changes; upregulation and downregulation of gene expression levels are indicated in red and blue shades, respectively, with darker colors indicating greater absolute fold-changes. Student's t-test PneumaCult™-ALI $vs.$ William's E, * ($p < 0.05$), ** ($p < 0.005$), and *** ($p < 0.0005$).

in Williams' E medium. PneumaCult-ALI™ medium contains several ingredients not present in William's E medium, such as insulin. Insulin acts as a chemoattractant for bronchial cells[42] and was shown to decrease the expression of pro-inflammatory proteins.[43] Insulin was also demonstrated to maintain albumin expression in mice.[44] The results thus demonstrated that the hepatic function of the HepaRG™ cells was retained when cultured for at least 10 days in PneumaCult-ALI™ medium.

Furthermore, to better understand how the coculture medium affects the HepaRG™ spheroids' metabolic capacity, we measured the expression of phase 1 metabolism-associated genes at days 1, 2, 3, 4, 7, and 10 of culturing. The expression of these genes in spheroids maintained in PneumaCult™-ALI medium was compared with that in spheroids cultured using the William's E medium, and fold-changes were calculated and visualized as a heatmap (Fig. 2e). The heatmap shows that the expression of many phase 1 metabolism-associated

genes was significantly altered in spheroids cultured in PneumaCult™-ALI compared with that in spheroids cultured in William's E medium. *CYP3A4* (>18-fold at day 10), *CYP3A43* (33-fold at day 2), and *CYP2B6* (>16-fold at day 10) were among the top upregulated genes ($p < 0.005$); *ALDH1A3* (10-fold at day 3), *CYP4A11* (nine-fold at day 3), and *ALDH3A1* (seven-fold at day 3) were among the top downregulated genes ($p < 0.005$). Most downregulated genes were affected during the first three days of culture, and expression levels mostly returned to levels seen in tissues maintained in William's E medium. The different composition of the PneumaCult-ALI™ compared with the William's E medium may explain these differences in gene expression. For example, hydrocortisone is an ingredient of PneumaCult™-ALI medium and a known inducer of CYP3A4.[45] Because the HepaRG™ spheroids remained viable and retained the expression of phase 1 metabolism-associated genes for 10 days, PneumaCult™-ALI medium was chosen as the NHBE ALI-HepaRG™ spheroid coculture medium.

Stability of the NHBE ALI or HepaRG™ spheroid monocultures-in-a-chip

We then tested the stability of the 3D NHBE ALI and HepaRG™ spheroid cultures, each individually cultured in the chip. We found that the HepaRG™ cells were strongly dependent on the medium volume available as tissues maintained in static or dynamic condition in a low medium volume always had a lower ATP content (ESI† Fig. S1). Two mechanisms could explain the relation between the spheroids' ATP content and the medium volume: first, the higher volume of cell culture medium probably increased the dilution of metabolic waste (*e.g.*, lactate, urea, CO_2, *etc.*), which could be critical for tissue viability in small volumes where waste levels can rise quickly (such as in static condition). Second, higher medium volumes possibly also improved nutrient availability, which might be particularly critical when several tissues are cocultured (as observed in the chip). To ensure optimal conditions for HepaRG™ spheroid long-term maintenance, a reservoir plate was connected to the chip to increase the volume of the circulating medium from 2.5 mL to 9 mL (Fig. 3a). Forty-eight mature spheroids, each composed of 12 500 HepaRG™ cells (corresponding to a total of 600 000 cells), were transferred to the liver compartment and maintained for 28 days in the fluidic plate with the PneumaCult™-ALI medium (Fig. 3a). Tissue viability, metabolic capacity, and functionality were evaluated on day 28.

Tissues in the chip exposed to medium flow (dynamic condition) had a similar morphology to tissues maintained in the standard spheroid microplate (static condition), with cells forming a dense tissue and a visible extracellular matrix (Fig. 3b). Nevertheless, tissues in the chip were smaller, suggesting partial cell loss, which was confirmed by an 18% decrease in ATP content compared with the static condition (Fig. 3c). To investigate that the metabolic capacity of HepaRG™ spheroids was retained when spheroids were cul-

tured in the chip, basal and TCDD-induced CYP1A1/1B1 activities were measured. The basal enzyme activity was low but comparable between the dynamic and static conditions (Fig. 3d). CYP1A1/1B1 activity was significantly induced by TCDD in both conditions ($p < 0.0005$) as expected, although enzyme induction in the spheroids cultured in dynamic conditions was only 40% of that in the HepaRG™ spheroids cultured in static conditions (Fig. 3d). This result was not expected, because shear stress caused by the medium flow was demonstrated previously to increase CYP1A1 activity.[46] As the assay we used to assess CYP activity detects a luminogenic substrate cleaved by the CYP1A1 present in the cells, cell loss over the extended maintenance period might partly explain the lower inducibility. We also measured the level of albumin, a protein secreted by mature hepatocytes[47] and a good indicator of hepatic function,[48] at every medium change. Secreted albumin levels were stable over the 28 days of culturing and were comparable between static and dynamic conditions (Fig. 3e). Albumin released by the HepaRG™ spheroids in static condition was significantly higher (on day 2) than the albumin levels released by tissues kept in dynamic condition. As this significant change was only observed on the first measurement, it could demonstrate that the tissues require at least two days to adapt to the medium flow. In both cases, secretion of albumin started to decrease on day 23, suggesting that tissue viability was decreasing after three weeks in culture. Together, these results demonstrate that HepaRG™ spheroids retained their functional characteristics when exposed to medium flow in the chip for 28 days.

Similar to the experiments performed using HepaRG™ spheroid cultures, the performance of the 3D NHBE ALI tissues that were maintained for 28 days in the chip exposed to medium flow (dynamic condition) was compared with that of the tissues maintained in a standard 24-well plate (static condition) for the same period. Two NHBE ALI tissues were placed in each circuit (one in the lung compartment and the other in the liver compartment), and the fluidic plate was connected to the reservoir plate to create conditions comparable to the HepaRG™ spheroid monoculture (Fig. 4a).

In comparison with HepaRG™ spheroid cultures, which were not affected by the chip material, the NHBE ALI tissues lost their tissue integrity when maintained for 7 days in polytetrafluoroethylene or polypropylene chips (ESI† Fig. S2). In contrast, the chip made from PEEK was biocompatible as the NHBE ALI tissues had a similar morphology to tissues maintained under static conditions even after 28 days of culture; tissues were pseudostratified, with the presence of goblet, ciliated, and basal cells (Fig. 4b). Tissues exposed to the medium flow also appeared slightly thinner. As previously demonstrated with osteoblasts[49] or C11-MDCK cells,[50] the shear stress caused by the medium flow could have decreased cell volume, thereby changing tissue thickness. While the shear stress caused by the medium flow might explain this observation,[51] there is currently no evidence that such mechanical stress across a porous membrane (10 μm thickness)
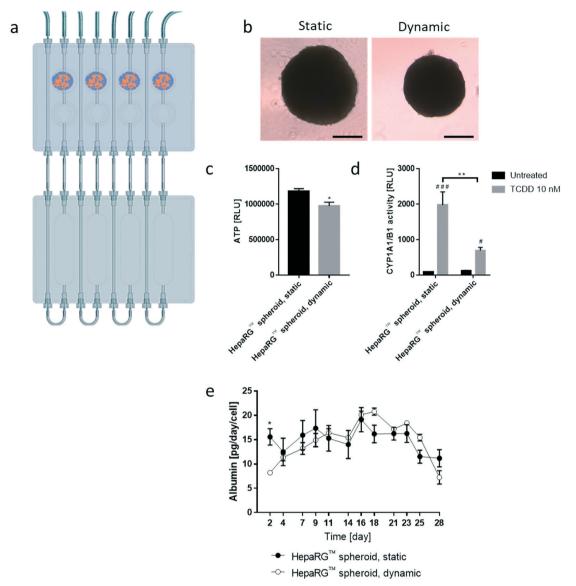
Fig. 3 Characterization of HepaRG™ spheroids maintained in the chip for 28 days. a) Scheme representing the fluidic plate connected to the reservoir plate. The four spheroid pictograms show the liver compartment where the 48 HepaRG™ spheroids were maintained for 28 days. b) Representative bright-field images of HepaRG™ spheroids maintained for 28 days in static (left; ultra-low adhesion microplate, no flow) or dynamic condition (right; chip, medium flow). Objective 10×. Scale bar: 200 μm. c) ATP content and d) basal and TCDD-induced CYP1A1/1B1 activity in both static and dynamic conditions on day 28. Data are presented as mean ± SEM of five independent measurements. RLU: relative light unit; TCDD: 2,3,7,8-tetrachlorodibenzodioxin. e) Albumin concentrations in the medium were quantified by ELISA at every medium change over the 28 day period. Data are presented as mean ± SEM of four independent measurements. Student's t-test HepaRG™ spheroid, dynamic vs. HepaRG™ spheroid, static * ($p < 0.05$), ** ($p < 0.005$), and *** ($p < 0.0005$). Student's t-test TCDD-treated vs. untreated, # ($p < 0.05$) and # # # ($p < 0.0005$).

could have affected the tissues. To better evaluate the distribution of ciliated and goblet cells in dynamic vs. static conditions, the NHBE ALI tissues were stained with antibodies targeting each cell type. We used a β-tubulin 4 antibody to detect the ciliated cells specifically; we observed that the cilia were distributed homogeneously in both conditions (Fig. 4c). Higher ciliogenesis in dynamic conditions was demonstrated in a previous study;[52] however, this was not observed here, most likely because the tissues used were already fully matured. MUC5AC staining was used to evaluate the presence of goblet cells, and our results demonstrated a homogenous dis-

tribution of goblet cells under both static and dynamic conditions (Fig. 4c). While the number of goblet cells was comparable, the signal of the MUC5AC-positive cells was weaker in dynamic than static cultures, suggesting less mucous substances in the goblet cells of the former.

The NHBE ALI tissues maintained in the chip for 28 days had a comparable morphology with tissues maintained under static conditions. Their comparable morphology also confirmed that the selected medium flow rate (150 μL min^{-1}) was appropriate for the NHBE ALI tissues. This flow rate was considered to not induce significant shear stress, which was

Fig. 4 Characterization of NHBE ALI tissues maintained in the chip for 28 days. a) Scheme representing the fluidic plate connected to the reservoir plate. The eight pictograms show the location of the eight NHBE ALI tissues maintained in the chip for 28 days. b) Representative histological sections of NHBE ALI tissues maintained under static (top; standard 24-well plate, no flow) or dynamic condition (bottom; chip, medium flow) for 28 days. Sections were stained with hematoxylin, eosin, and Alcian blue. Magnification: 20×. c) Representative images of β-tubulin 4- (green) and MUC5AC (yellow)-stained NHBE ALI tissues maintained under static or dynamic conditions for 28 days. Nuclei were counterstained with DAPI (blue). BTUB4: β-tubulin 4; MUC5AC: mucin 5AC. Magnification: 20×. Scale bar: 400 μm. d) TEER and e) CBF were measured in NHBE ALI tissues maintained in static or dynamic conditions for 28 days. Data are presented as mean ± SEM for seven independent measures. Student's t-test NHBE ALI, static vs. dynamic *** ($p < 0.0005$).

reported to trigger morphological abnormalities due to cytoskeletal reorganization in human renal proximal tubular cells.[50]

Furthermore, NHBE ALI tissue functionality was assessed based on two measures: TEER and CBF. TEER, a marker of tight junction integrity,[51] increased by ~50% in all NHBE ALI tissues maintained in the chip under medium flow (NHBE ALI, dynamic) compared with the static condition (Fig. 4d). A similar observation was made previously with NHBE ALI and

small airway tissues exposed to medium flow.[52] As mentioned previously, there is currently no evidence that the shear stress can act across the porous membrane. Cilia beating, a key mechanism for mucociliary clearance and defense of the airways against inhaled particles and pathogens,[53] was also monitored in NHBE ALI tissues. The CBF of NHBE ALI samples was not impacted by the flow condition (Fig. 4e). This result not only demonstrated the functionality of ciliated cells but also suggested that mucus viscosity, number of cilia,

and length of cilia – three factors known to affect CBF[54] – remained unchanged.

Assessment of lung-liver crosstalk in the chip

To evaluate the effects of the NHBE ALI tissues-HepaRG™ spheroids crosstalk, we cocultured one NHBE ALI tissue (NHBE ALI, coculture condition) and a total of 600 000 HepaRG™ cells (48 spheroids × 12 500 cells; HepaRG™ spheroid, coculture condition; Fig. 5) in each circuit. PneumaCult™-ALI medium was used as coculture medium. Tissues were maintained for a total of 28 days in the chip be-

fore evaluating their morphology, functionality, and metabolic capacity. Morphology of the NHBE ALI tissues cocultured with the HepaRG™ spheroids under flow (Fig. 5b) was similar to that of tissues maintained in static conditions (Fig. 5b); the NHBE ALI tissues exhibited pseudostratified organization comprising basal, goblet, and ciliated cells. As previously observed with NHBE ALI tissues in monoculture, the NHBE ALI tissues in coculture were thinner than the tissues in static condition CBF (Fig. 5c), and TEER (Fig. 5d) in NHBE ALI tissues cocultured with HepaRG™ spheroids were similar to those obtained for tissues maintained in chip monoculture (NHBE ALI, dynamic condition). When cocultured with NHBE
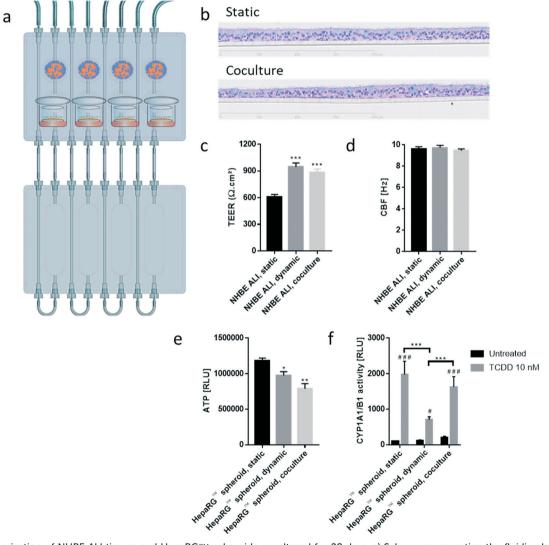

Fig. 5 Characterization of NHBE ALI tissues and HepaRG™ spheroids cocultured for 28 days. a) Scheme representing the fluidic plate connected to the reservoir plate. The pictograms show the location of the different tissues in the chip. b) Representative histological sections of NHBE ALI tissues maintained in static (top; standard multi-well plate, no flow) or coculture conditions (bottom; chip, medium flow) for 28 days. Tissue sections were stained with hematoxylin, eosin, and Alcian blue. Magnification: 20×. c) TEER and d) CBF were measured in NHBE ALI tissues maintained in static, dynamic, or coculture conditions for 28 days. e) ATP content in single HepaRG™ spheroids maintained in static, dynamic, or coculture conditions was measured on day 28. f) Basal and TCDD-induced CYP1A1/1B1 activities were measured per HepaRG™ spheroid maintained in static, dynamic, or coculture conditions for 28 days. RLU: relative light unit; TCDD: 2,3,7,8-tetrachlorodibenzodioxin. Data are presented as mean ± SEM of five independent measurements. Student's t-test comparing NHBE ALI, static vs. NHBE ALI, dynamic or NHBE ALI, coculture, and HepaRG™ spheroid, static vs. HepaRG™ spheroid, dynamic or HepaRG™ spheroid, coculture, * ($p < 0.05$), ** ($p < 0.005$), and *** ($p < 0.0005$). Student's t-test TCDD-treated vs. untreated, # ($p < 0.05$) and # # # ($p < 0.0005$).

ALI tissues, the ATP levels of HepaRG™ spheroids were reduced by 20% compared with HepaRG™ spheroids in monoculture and by 34% compared with HepaRG™ spheroids maintained in static conditions (Fig. 5e). In addition, CYP1A1/1B1 basal activity was ~85% higher in the cocultured condition in comparison with HepaRG™ spheroids in monoculture or static condition. The CYP1A1/1B1 inducibility was also improved in HepaRG™ spheroids cocultured with NHBE ALI tissues in the chip compared with HepaRG™ spheroids in monoculture (Fig. 5f). As explained previously, HepaRG™ cells are particularly sensitive to the volume of medium, possibly because it directly affects the concentration of metabolic waste or because nutrient availability is lower; NHBE ALI tissues might have released metabolic waste or consumed some of the available nutrients, causing the ATP content of the HepaRG™ spheroids to decrease when NHBE ALI tissues are present. The higher CYP1A1/1B1 activity measured in HepaRG™ spheroids cocultured with NHBE ALI tissues could be explained by the secretion of factors from the latter that

may have an impact on HepaRG™ cell function. For example, the hepatocyte nuclear factor 4α, a key protein regulating multiple genes including CYP1A1/1B1 expression,[55] is also regulated by numerous cofactors and compounds[56] that could possibly be released by the NHBE ALI tissues.

Taken together, these results demonstrate the viability of both tissues in coculture with the maintenance of key bronchial and hepatic markers over the experimental period.

To better evaluate the impact of coculturing both tissues in the same circuit, we measured glucose, lactate, and albumin concentrations in the medium at various time points during the 28 day culture. The values for the medium of the cocultures were compared with those obtained for the medium from HepaRG™ spheroids maintained as monoculture in dynamic conditions (Fig. 3e). Between days 2 and 7, albumin levels in the medium were around 15 pg per day per HepaRG™cell, independent of culture condition (Fig. 6a). Between days 9 and 14, a significant increase in albumin levels was observed in the medium of the cocultures

Fig. 6 Levels of a) albumin, b) glucose, and c) lactate in the media during 28 day culture. Measurements of albumin, glucose, and lactate concentrations were performed every two or three days, and results for the HepaRG™ dynamic monoculture (HepaRG™ spheroid, dynamic) and NHBE ALI-HepaRG™ spheroid coculture (coculture) conditions were compared. In addition, glucose concentrations were monitored in the stock medium. Data are presented as mean ± SEM of four independent measurements. Student's t-test coculture $vs.$ HepaRG™ spheroid, dynamic, * ($p < 0.05$), ** ($p < 0.005$), and *** ($p < 0.0005$).

compared with those in the medium of the HepaRG™ spheroid monoculture. From day 14, the albumin secretion in the cocultures decreased slightly but remained stable. The slightly higher secretion of albumin detected in the medium of the coculture could confirm our hypothesis that the NHBE ALI tissues might have changed the coculture medium composition by consuming or releasing factors that resulted in improved HepaRG™ spheroid functionality. Throughout the 28-day culture, we detected stable glucose concentrations between 15 and 17 mM, independent of the mode of HepaRG™ spheroid culture (*i.e.*, monoculture or coculture) (Fig. 6b). The concentration of lactate, which is dependent on glucose metabolization, was significantly higher in the medium of the cocultures than in the medium of the HepaRG™ monoculture (Fig. 6c). However, it was in the range of physiological lactate concentrations, which averages around 1 mM in blood.[57] The higher concentrations of lactate in the coculture medium supported the notion that the NHBE cells actively metabolized the glucose present in the medium. Because differences in glucose levels were not observed between the two conditions, these results suggest that the HepaRG™ spheroids utilize lactate to synthesize glucose *de novo*, as previously reported.[38] Together, these results demonstrate that the NHBE ALI tissues and HepaRG™ spheroids cocultures were stable in the chip for 28 days.

Assessment of AFB1 toxicity using the lung/liver-on-a-chip

To further demonstrate the crosstalk between the NHBE ALI tissues and the HepaRG™ spheroids in the chip, we exposed NHBE ALI tissues to AFB1 with and without coculture with HepaRG™ spheroids. We consider that the lung/liver-on-a-chip platform is suitable to study the toxicity of AFB1, because the HepaRG™ liver model was demonstrated to metabolize AFB1 similarly to primary human hepatocytes, HepG2, and HepaRG™ cells.[28]

AFB1 is a mycotoxin produced by *Aspergillus flavus* and a common food contaminant in warm and humid countries.[58] AFB1 is mainly known as a hepatocarcinogen[59] but is also cytotoxic for the brain vasculature[60] and the kidney.[61] Several studies showed that AFB1 can cause lung carcinoma[62] and induce lung cytotoxicity.[63,64] The metabolization of AFB1 by several CYP enzymes to activated or detoxified metabolites may contribute to the organ-specific toxicity of this compound. In the lung, three main enzymes bioactivate AFB1 and generate cytotoxic metabolites, including CYP1A2 and 3A4, both of which transform AFB1 into AFB1-8,9-epoxide (AFBO),[65] and CYP2A13, which transforms AFB1 into AFBO and/or aflatoxin M1-8,9-epoxide (AFM1).[66,67] Both AFM1 and AFBO were demonstrated to be cytotoxic.[63,68] In the liver, AFB1 is metabolized mainly by CYP1A2 and 3A4, forming three major metabolites: AFBO, AFM1, and aflatoxin Q1 (AFQ1).[67] The liver might thus play an essential role in decreasing the AFB1 toxicity, because it can metabolize the parent compound AFB1 to AFQ1, which is considered a detoxification product.[69]

To detect cytotoxic effects of ABF1 in a short period (<72 hours) using our chip platform, we exposed NHBE ALI tissues

and HepaRG™ spheroids to a high concentration (100 μM) of AFB1. NHBE ALI tissues in monoculture (NHBE ALI, dynamic) showed signs of severe cytotoxicity after 48 hours, with a significantly decreased TEER (Fig. 7a) and a slightly lower ATP content (Fig. 7b) compared with untreated NHBE ALI tissues maintained in static condition (NHBE ALI, static, untreated). After 72 hours of exposure, TEER reached a value similar to that of an empty insert, and ATP content was significantly decreased compared with that of untreated NHBE ALI tissues (in static condition) ($p < 0.005$). NHBE ALI tissues cocultured with HepaRG™ spheroids exhibited a response with a different kinetic; tissues were unaffected by the mycotoxin for the first 48 hours, before TEER values decreased at 72 hours of exposure (Fig. 7a). The ATP content in NHBE ALI tissues connected to the HepaRG™ spheroids (NHBE ALI, coculture) remained similar to that of untreated tissues in static conditions at both time points (Fig. 7b). Although the high cytotoxicity of AFB1 in the NHBE ALI tissues could be caused by AFB1 itself, the cytotoxicity was more likely

Fig. 7 AFB1 toxicity was assessed using the lung/liver-on-a-chip. a) TEER and b) ATP content were measured in untreated or AFB1-exposed NHBE ALI tissues either in monoculture (NHBE ALI, dynamic) or coculture with HepaRG™ spheroids (NHBE ALI, coculture). c) ATP content in untreated (HepaRG™ spheroid, static, untreated) or AFB1-exposed, cocultured HepaRG™ spheroids (HepaRG™ spheroid, coculture). Data are presented as mean ± SEM of eight independent measurements. Student's *t*-test *vs.* static untreated, ** ($p < 0.005$) and *** ($p < 0.0005$).

attributed to its metabolites AFBO or AFM1, because NHBE ALI tissues express CYP1A2 and CYP2A13,[70] which are responsible for the generation of AFBO and AFM1, respectively. The delayed cytotoxicity in NHBE ALI tissues cocultured with HepaRG™ spheroids suggests that at least a part of the AFB1 was transformed into a less toxic metabolite. Based on the earlier observation of high CYP3A4 expression in the HepaRG™ spheroids maintained in PneumaCult-ALI™ medium (Fig. 2d), we could argue that AFB1 was transformed into AFQ1, thus decreasing the amount of cytotoxic metabolites circulating in the chip. HepaRG™ spheroids maintained in the chip and exposed to AFB1 had significantly impaired viability after 48 and 72 hours, confirming the hepatic cytotoxicity of ABF1 ($p < 0.0005$) (Fig. 7c).

Conclusions

The lung/liver-on-a-chip presented here offers a new approach to assess the potential toxicity of inhaled compounds. Previously demonstrated lung culture systems focused on the functionality and physical properties of the lung tissue (*e.g.*, mimicking the epithelial stretching during breathing[9,11]). Our work focused on the lung–liver connection not only to better evaluate the effects of the metabolized compound on the lung but also to demonstrate the potential impact of inhaled compounds on the liver. Compared with various chip models already described in the literature, our system is practical to use; it can be maintained in an incubator with simple arrangement, it is a standard 24-well plate format, and it is easy to connect and disconnect from the pump. Also, the chip enables circulation of a higher medium volume, which is beneficial to provide tissues with nutrients and remove waste. The use of an open architecture ensures optimal gas exchanges among the tissues, the medium, and the surrounding air. The open architecture also keeps the level of medium stable in each circuit. Having a user-friendly platform in a macroformat markedly decreases the probability of technical issues (*e.g.*, air bubbles that are often formed in microformat systems, which may easily block the flow of media). Finally, the current chip offers one critical advantage compared to previously described chips: it is suitable for testing drug efficacy and safety, because we chose to use a non-absorbent material.

Furthermore, the use of physiologically relevant models, such as the 3D NHBE ALI and HepaRG™ spheroid models, closely mimics the human organ functions better than simpler two-dimensional submerged culture models. We demonstrated that the platform is functional and retains the metabolic activity of both organs for 28 days. A chip combining lung and liver tissues, facilitating viability of both tissues for 14 days, was described previously.[71] That system allowed for a precise control of medium flow using electromagnetic actuators. While our chip does not offer such an extended level of flow control, the specificities of our chip (material, ease of use, volume of medium) have contributed to the unprecedented duration of NHBE ALI tissues and HepaRG™ spher-

oid maintenance within the chip. In the future, the system can be modified to combine more organs.

Moreover, several aspects of the platform can be improved, including the formulation of an alternative coculture medium, other liver models, and increased throughput. Currently, a cell culture medium adapted for the maintenance of any cell type does not exist. In consequence, connecting multiple *in vitro* models of different organs is limited to the availability of the culture medium that would be suitable for all. With our MOC, we observed several adverse effects of the medium on HepaRG™ spheroid viability that could be attributed to the glucose level. Adapting the glucose concentration will be further tested in the future. A custom-made medium optimized for both tissues could be developed and tested for the chip, as described previously.[71] We acknowledge that although the HepaRG™ spheroids used for the chip are a good human hepatocyte surrogate, other liver cells may be equally useful. The human liver comprises hepatocytes, biliary, hepatic stellate, and Kupffer cells. Hepatic stellate and Kupffer cells both play a role in the immune defense of the liver and have essential roles in the pathophysiology of liver fibrosis, hepatitis, or steatohepatitis.[72,73] Therefore, for testing the efficacy of drugs, for example, the *in vivo* human liver responses may be more adequately simulated in liver models containing these cell types.

The lung/liver-on-a-chip platform described here was demonstrated to be suitable for the assessment of compound toxicity. The platform will be equally useful for testing other compounds administered differently (*e.g.*, mimicking the inhalation route). Appropriate *in vitro* exposure systems, such as the Vitrocell® Exposure System,[74] can be used to expose ALI cultures to various aerosols or aerosol mixtures.[75,76] The bioavailability of potential drugs administered *via* various routes could be tested using the platform and potentially lead to the development of new entry routes for existing drugs (*e.g.*, as in the case of insulin).[77,78] As NHBE ALI tissues can also be prepared using cells from diseased donors (asthma[79] or COPD[80]), the use of such tissues in the chip could help further the development of safer and more effective drugs for those diseases. The use of such a platform is aligned with the 3R principles of replacing, reducing, and refining the use of animals and will undoubtedly provide higher sensitivity in detecting potential toxicity of new drugs and therapeutics than the use of traditional monoculture and submerged culture models.

Conflicts of interest

Acknowledgements

greatly assisted this research. The authors would like to acknowledge the following individuals for contributing their technical expertise: Moran Morelli for the cell culture; Camille Schilt, Anaelle Dubois, and Marie Sgandurra for histology; Dariusz Peric for RNA purification; Remi Dulize and David Bornand for microarray experiments; Stephanie Boue for providing illustrations of the different tissue types.

Part of this work was presented at the Tenth World Congress on Alternatives and Animal Use in the Life Sciences (WA, USA) from August 20–24, 2017.

References

1 O. K. Kurt, J. Zhang and K. E. Pinkerton, Pulmonary health effects of air pollution, *Curr. Opin. Pulm. Med.*, 2016, **22**, 138–143.

2 M. I. Gilmour, M. Daniels and R. C. McCrillis, *et al.*, Air pollutant-enhanced respiratory disease in experimental animals, *Environ. Health Perspect.*, 2001, **109**(Suppl 4), 619–622.

3 M. Martignoni, G. M. M. Groothuis and R. de Kanter, Species differences between mouse, rat, dog, monkey and human CYP-mediated drug metabolism, inhibition and induction, *Expert Opin. Drug Metab. Toxicol.*, 2006, **2**, 875–894.

4 N. Alépée, A. Bahinski and M. Daneshian, *et al.* State-of-the-art of 3D cultures (organs-on-a-chip) in safety testing and pathophysiology, *ALTEX*, 2014, **31**, 441–477.

5 P. H. Karp, T. O. Moninger and S. P. Weber, *et al.*, An in vitro model of differentiated human airway epithelia. Methods for establishing primary cultures, *Methods Mol. Biol.*, 2002, **188**, 115–137.

6 B. Leclercq, M. Happillon and S. Antherieu, *et al.*, Differential responses of healthy and chronic obstructive pulmonary diseased human bronchial epithelial cells repeatedly exposed to air pollution-derived PM4, *Environ. Pollut.*, 2016, **218**, 1074–1088.

7 T. M. Krunkosky, J. L. Jordan and E. Chambers, *et al.* Mycoplasma pneumoniae host–pathogen studies in an air–liquid culture of differentiated human airway epithelial cells, *Microb. Pathog.*, 2007, **42**, 98–103.

8 D. Bovard, A. Iskandar and K. Luettich, *et al.* Organs-on-a-chip: A new paradigm for toxicological assessment and preclinical drug development, *Toxicol. Res. Appl.*, 2017, **1**, DOI: 10.1177/2397847317726351.

9 D. D. Huh, A Human Breathing Lung-on-a-Chip, *Ann. Am. Thorac. Soc.*, 2015, **12**, S42–S44.

10 K. H. Benam, R. Villenave and C. Lucchesi, *et al.* Small airway-on-a-chip enables analysis of human lung inflammation and drug responses in vitro, *Nat. Methods*, 2016, **13**, 151–157.

11 A. O. Stucki, J. D. Stucki and S. R. R. Hall, *et al.* A lung-on-a-chip array with an integrated bio-inspired respiration mechanism, *Lab Chip*, 2015, **15**, 1302–1310.

12 J. Y. Zhang, Y. Wang and C. Prakash, Xenobiotic-metabolizing enzymes in human lung, *Curr. Drug Metab.*, 2006, **7**, 939–948.

13 U. M. Zanger and M. Schwab, Cytochrome P450 enzymes in drug metabolism: Regulation of gene expression, enzyme activities, and impact of genetic variation, *Pharmacol. Ther.*, 2013, **138**, 103–141.

14 U. Marx, T. Andersson, A. Bahinski, M. Beilmann, S. Beken, F. Cassee, M. Cirit, M. Daneshian, S. Fitzpatrick, O. Frey, C. Gaertner, C. Giese, L. Griffith, T. Hartung, M. Heringa, J. Hoeng, W. de Jong, H. Kojima, J. Kuehnl, M. Leist, A. Luch, I. Maschmeyer, D. Sakharov, A. Sips, T. Steger-Hartmann, D. Tagle, A. Tonevitsky, T. Tralau, S. Tsyb, A. van de Stolpe, R. Vandebriel, P. Vulto, J. Wang, J. Wiest, M. Rodenburg and A. Roth, Biology-inspired microphysiological system approaches to solve the prediction dilemma of substance testing, *ALTEX - Altern. Anim. Ex.*, 2016, **33**(3), 272–321.

15 E. M. Materne, I. Maschmeyer, A. K. Lorenz, R. Horland, K. M. Schimek, M. Busek, F. Sonntag, R. Lauster and U. Marx, The multi-organ chip – a microfluidic platform for long-term multi-tissue coculture, *J. Visualized Exp.*, 2015, (98), e52526.

16 S. Lee and J. Sung, Microtechnology-Based Multi-Organ Models, *Bioengineering*, 2017, **4**, 46.

17 I. Maschmeyer, A. K. Lorenz and K. Schimek, *et al.*, A four-organ-chip for interconnected long-term co-culture of human intestine, liver, skin and kidney equivalents, *Lab Chip*, 2015, **15**, 2688–2699.

18 A. Choe, S. K. Ha and I. Choi, *et al.*, Microfluidic Gut-liver chip for reproducing the first pass metabolism, *Biomed. Microdevices*, 2017, **19**, 4.

19 C. Oleaga, C. Bernabini and A. S. Smith, *et al.* Multi-Organ toxicity demonstration in a functional human in vitro system composed of four organs, *Sci. Rep.*, 2016, **6**, 20030.

20 A. S. Kalgutkar, Role of Bioactivation in Idiosyncratic Drug Toxicity: Structure–Toxicity Relationships, in *Advances in Bioactivation Research*, ed. A. Elfarra, Springer, New York, NY, 2008, pp. 1–29.

21 P. Godoy, N. J. Hewitt and U. Albrecht, *et al.* Recent advances in 2D and 3D in vitro systems using primary hepatocytes, alternative hepatocyte sources and non-parenchymal liver cells and their use in investigating mechanisms of hepatotoxicity, cell signaling and ADME, *Arch. Toxicol.*, 2013, **87**, 1315–1530.

22 P. Gunness, D. Mueller and V. Shevchenko, *et al.* 3D organotypic cultures of human HepaRG cells: a tool for in vitro toxicity studies, *Toxicol. Sci.*, 2013, **133**, 67–78.

23 C. C. Bell, D. F. G. Hendriks and S. M. L. Moro, *et al.*, Characterization of primary human hepatocyte spheroids as a model system for drug-induced liver injury, liver function and disease, *Sci. Rep.*, 2016, **6**, 25187.

24 I. Wagner, E.-M. Materne and S. Brincker, *et al.*, A dynamic multi-organ-chip for long-term cultivation and substance testing proven by 3D human liver and skin tissue co-culture, *Lab Chip*, 2013, **13**, 3538.

25 Y. Takahashi, Y. Hori, T. Yamamoto, T. Urashima, Y. Ohara and H. Tanaka, 3D spheroid cultures improve the metabolic gene expression profiles of HepaRG cells, *Biosci. Rep.*, 2015, **35**(3), e00208.

26 A. Mann, T. Pelz and K. Rennert, *et al.* Evaluation of HepaRG cells for the assessment of indirect drug-induced

hepatotoxicity using INH as a model substance, *Hum. Cell*, 2017, **30**, 267–278.

27 M. R. McGill, H.-M. Yan and A. Ramachandran, *et al.* HepaRG cells: A human model to study mechanisms of acetaminophen hepatotoxicity, *Hepatology*, 2011, **53**, 974–982.

28 Y. Yokoyama, Y. Sasaki and N. Terasaki, *et al.* Comparison of Drug Metabolism and Its Related Hepatotoxic Effects in HepaRG, Cryopreserved Human Hepatocytes, and HepG2 Cell Cultures, *Biol. Pharm. Bull.*, 2018, **41**, 722–732.

29 A. R. Iskandar, Y. Xiang and S. Frentzel, *et al.* Impact Assessment of Cigarette Smoke Exposure on Organotypic Bronchial Epithelial Tissue Cultures: A Comparison of Mono-Culture and Coculture Model Containing Fibroblasts, *Toxicol. Sci.*, 2015, **147**, 207–221.

30 S. Chortarea, M. J. D. Clift and D. Vanhecke, *et al.* Repeated exposure to carbon nanotube-based aerosols does not affect the functional properties of a 3D human epithelial airway model, *Nanotoxicology*, 2015, **9**, 983–993.

31 A. Schmid, N. Baumlin and P. Ivonnet, *et al.* Roflumilast partially reverses smoke-induced mucociliary dysfunction, *Respir. Res.*, 2015, **16**, 135.

32 G. Damera, H. Zhao and M. Wang, *et al.* Ozone modulates IL-6 secretion in human airway epithelial and smooth muscle cells, *Am. J. Physiol.*, 2009, **296**, L674–L683.

33 S. M. Kurtz and J. N. Devine, PEEK biomaterials in trauma, orthopedic, and spinal implants, *Biomaterials*, 2007, **28**, 4845–4869.

34 J. D. Wang, N. J. Douville and S. Takayama, *et al.* Quantitative Analysis of Molecular Absorption into PDMS Microfluidic Channels, *Ann. Biomed. Eng.*, 2012, **40**, 1862–1873.

35 M. W. Toepke and D. J. Beebe, PDMS absorption of small molecules and consequences in microfluidic applications, *Lab Chip*, 2006, **6**, 1484.

36 *Drug addiction: from basic research to therapy*, ed. R. S. Rapaka and W. Sadée, Springer, New York, NY, 2008.

37 K. J. Livak and T. D. Schmittgen, Analysis of Relative Gene Expression Data Using Real-Time Quantitative PCR and the 2−∆∆CT Method, *Methods*, 2001, **25**, 402–408.

38 C. H. Samanez, S. Caron and O. Briand, *et al.* The human hepatocyte cell lines IHH and HepaRG: models to study glucose, lipid and lipoprotein metabolism, *Arch. Physiol. Biochem.*, 2012, **118**, 102–111.

39 J. M. Berg, J. L. Tymoczko and L. Stryer, *et al. Biochemistry*, W. H. Freeman, New York, NY, 5th edn, 2002, ch. 4 print.

40 F. K.-M. Chan, K. Moriwaki and M. J. De Rosa, Detection of Necrosis by Release of Lactate Dehydrogenase Activity, in *Immune Homeostasis*, ed. A. L. Snow and M. J. Lenardo, Humana Press, Totowa, NJ, 2013, pp. 65–70.

41 B. J. Altman and J. C. Rathmell, Metabolic Stress in Autophagy and Cell Death Pathways, *Cold Spring Harbor Perspect. Biol.*, 2012, **4**, a008763.

42 S. Shoji, R. F. Ertl and J. Linder, *et al.* Bronchial Epithelial Cells Respond to Insulin and Insulin-like Growth Factor-I as a Chemoattractant, *Am. J. Respir. Cell Mol. Biol.*, 1990, **2**, 553–557.

43 V. D. Gandhi, N. Shrestha Palikhe and S. M. Hamza, *et al.* Insulin decreases expression of the proinflammatory receptor proteinase-activated receptor-2 on human airway epithelial cells, *J. Allergy Clin. Immunol.*, 2018, **142**(3), 1003–1006.

44 Q. Chen, M. Lu and B. R. Monks, *et al.* Insulin Is Required to Maintain Albumin Expression by Inhibiting Forkhead Box O1 Protein, *J. Biol. Chem.*, 2016, **291**, 2371–2378.

45 W. El-Sankary, N. J. Plant and G. G. Gibson, *et al.* Regulation of the CYP3A4 gene by hydrocortisone and xenobiotics: role of the glucocorticoid and pregnane X receptors, *Drug Metab. Dispos.*, 2000, **28**, 493–496.

46 Z. Han, Y. Miwa and H. Obikane, *et al.* Aryl hydrocarbon receptor mediates laminar fluid shear stress-induced CYP1A1 activation and cell cycle arrest in vascular endothelial cells, *Cardiovasc. Res.*, 2007, **77**, 809–818.

47 X. Ma, Y. Duan and C. J. Jung, *et al.* The Differentiation of Hepatocyte-Like Cells from Monkey Embryonic Stem Cells, *Cloning Stem Cells*, 2008, **10**, 485–494.

48 R. Spinella, R. Sawhney and R. Jalan, Albumin in chronic liver disease: structure, functions and therapeutic implications, *Hepatol. Int.*, 2016, **10**, 124–132.

49 L. Liu, S. Cai and G. Qiu, *et al.* Fluid shear stress enhances the cell volume decrease of osteoblast cells by increasing the expression of the ClC-3 chloride channel, *Biomed. Rep.*, 2016, **4**, 408–412.

50 D. Maggiorani, R. Dissard and M. Belloy, *et al.* Shear Stress-Induced Alteration of Epithelial Organization in Human Renal Tubular Cells, *PLoS One*, 2015, **10**, e0131416.

51 B. Srinivasan, A. R. Kolli and M. B. Esch, *et al.* TEER Measurement Techniques for In Vitro Barrier Model Systems, *J. Lab. Autom.*, 2015, **20**, 107–126.

52 P. Chandorkar, W. Posch and V. Zaderer, *et al.* Fast-track development of an in vitro 3D lung/immune cell model to study Aspergillus infections, *Sci. Rep.*, 2017, **7**(1), 11644.

53 J. D. Londino, J. F. Collawn and S. Matalon Regulation of Airway Lining Fluid in Health and Disease, in *Comparative Biology of the Normal Lung*, Elsevier, 2015, pp. 467–477.

54 W. L. Lee, P. G. Jayathilake and Z. Tan, *et al.* Muco-ciliary transport: Effect of mucus viscosity, cilia beat frequency and cilia density, *Comput. Fluids*, 2011, **49**, 214–221.

55 C. P. Martinez-Jimenez, J. V. Castell and M. J. Gomez-Lechon, *et al.* Transcriptional Activation of CYP2C9, CYP1A1, and CYP1A2 by Hepatocyte Nuclear Factor 4 Requires Coactivators Peroxisomal Proliferator Activated Receptor-Coactivator 1 and Steroid Receptor Coactivator 1, *Mol. Pharmacol.*, 2006, **70**, 1681–1692.

56 C. Chen, A. Soto-Gutierrez and P. M. Baptista, *et al.* Biotechnology Challenges to In Vitro Maturation of Hepatic Stem Cells, *Gastroenterology*, 2018, **154**, 1258–1272.

57 M. L. Goodwin, J. E. Harris and A. Hernández, *et al.* Blood Lactate Measurements and Analysis during Exercise: A Guide for Clinicians, *J. Diabetes Sci. Technol.*, 2007, **1**, 558–569.

58 P. L. Foster and W. A. Rosche Aflatoxins, in *Encyclopedia of Genetics*, Elsevier, 2001, pp. 20–21.

59 M. Kew, Hepatocellular carcinoma: epidemiology and risk factors, *J. Hepatocell. Carcinoma*, 2014, 115.

60 H. Qureshi, S. S. Hamid and S. S. Ali, *et al.* Cytotoxic effects of aflatoxin B1 on human brain microvascular endothelial cells of the blood-brain barrier, *Med. Mycol.*, 2015, **53**, 409–416.

61 J. Theobald, A. Ghanem and P. Wallisch, *et al.* Liver-Kidney-on-Chip To Study Toxicity of Drug Metabolites, *ACS Biomater. Sci. Eng.*, 2018, **4**, 78–89.

62 J. D. Kelly, D. L. Eaton and F. P. Guengerich, *et al.* Aflatoxin B1Activation in Human Lung, *Toxicol. Appl. Pharmacol.*, 1997, **144**, 88–95.

63 T. Palanee, M. F. Dutton and A. A. Chuturgoon, Cytotoxicity of aflatoxin B1 and its chemically synthesised epoxide derivative on the A549 human epithelioid lung cell line, *Mycopathologia*, 2001, **151**, 155–159.

64 T. R. V. Vleet, P. J. Klein and R. A. Coulombe Jr, Metabolism and cytotoxicity of Aflatoxin B1 in cytochrome P-450-expressing human lung cells, *J. Toxicol. Environ. Health, Part A*, 2001, **63**, 525–540.

65 T. R. Van Vleet, K. Macé and R. A. Coulombe, Comparative aflatoxin B(1) activation and cytotoxicity in human bronchial cells expressing cytochromes P450 1A2 and 3A4, *Cancer Res.*, 2002, **62**, 105–112.

66 X.-Y. He, L. Tang and S.-L. Wang, *et al.* Efficient activation of aflatoxin B1 by cytochrome P450 2A13, an enzyme predominantly expressed in human respiratory tract, *Int. J. Cancer*, 2006, **118**, 2665–2671.

67 V. Dohnal, Q. Wu and K. Kuča, Metabolism of aflatoxins: key enzymes and interindividual as well as interspecies differences, *Arch. Toxicol.*, 2014, **88**, 1635–1644.

68 J. Bujons, D. P. Hsieh and N. Y. Kado, *et al.* Aflatoxin M1 8,9-epoxide: preparation and mutagenic activity, *Chem. Res. Toxicol.*, 1995, **8**, 328–332.

69 D. P. H. Hsieh, A. S. Salhab and J. J. Wong, *et al.* Toxicity of aflatoxin Q1 as evaluated with the chicken embryo and bacterial auxotrophs, *Toxicol. Appl. Pharmacol.*, 1974, **30**, 237–242.

70 N. Newland, A. Baxter and K. Hewitt, *et al.* CYP1A1/1B1 and CYP2A6/2A13 activity is conserved in cultures of differentiated primary human tracheobronchial epithelial cells, *Toxicol. In Vitro*, 2011, **25**, 922–929.

71 J. R. Coppeta, M. J. Mescher and B. C. Isenberg, *et al.* A portable and reconfigurable multi-organ platform for drug development with onboard microfluidic flow control, *Lab Chip*, 2017, **17**, 134–144.

72 G. Kolios, V. Valatas and E. Kouroumalis, Role of Kupffer cells in the pathogenesis of liver disease, *World J. Gastroenterol.*, 2006, **12**, 7413–7420.

73 M. L. Hautekeete and A. Geerts, The hepatic stellate (Ito) cell: its role in human liver disease, *Virchows Arch.*, 1997, **430**, 195–207.

74 D. Thorne and J. Adamson, A review of in vitro cigarette smoke exposure systems, *Exp. Toxicol. Pathol.*, 2013, **65**, 1183–1193.

75 M. Röhm, S. Carle and F. Maigler, *et al.* A comprehensive screening platform for aerosolizable protein formulations for intranasal and pulmonary drug delivery, *Int. J. Pharm.*, 2017, **532**, 537–546.

76 S. Majeed, S. Frentzel and S. Wagner, *et al.* Characterization of the Vitrocell® 24/48 in vitro aerosol exposure system using mainstream cigarette smoke, *Chem. Cent. J.*, 2014, **8(1)**, 62.

77 L. D. Mastrandrea, Inhaled insulin: overview of a novel route of insulin administration, *Vasc. Health Risk Manage.*, 2010, **6**, 47–58.

78 J. S. Patton and P. R. Byron, Inhaling medicines: delivering drugs to the body through the lungs, *Nat. Rev. Drug Discovery*, 2007, **6**, 67–74.

79 D. Gras, A. Bourdin and I. Vachier, *et al.* An ex vivo model of severe asthma using reconstituted human bronchial epithelium, *J. Allergy Clin. Immunol.*, 2012, **129**, 1259–1266.e1.

80 G. D. Amatngalim, J. A. Schrumpf and A. Henic, *et al.* Antibacterial Defense of Human Airway Epithelial Cells from Chronic Obstructive Pulmonary Disease Patients Induced by Acute Exposure to Nontypeable Haemophilus influenzae: Modulation by Cigarette Smoke, *J. Innate Immun.*, 2017, **9**, 359–374.